

# Shortest Path Distance in Manhattan Poisson Line Cox Process

Vishnu Vardhan Chetlur, Harpreet S. Dhillon, Carl P. Dettmann

## Abstract

While the Euclidean distance characteristics of the Poisson line Cox process (PLCP) have been investigated in the literature, the analytical characterization of the path distances is still an open problem. In this paper, we characterize the length of the shortest path between the typical point and its nearest neighbor in the sense of path distance in a stationary Manhattan Poisson line Cox process (MPLCP), which is a variant of the PLCP. First, we derive the exact cumulative distribution function (CDF) of the length of the shortest path for the typical point at an intersection to its nearest neighbor in the sense of path distance. Further, we derive an upper bound and a remarkably accurate but approximate lower bound on the CDF of the shortest path distance for the typical point at an arbitrary position. We also discuss the application of these results in infrastructure planning, wireless communication, and transportation networks.

## Index Terms

Stochastic geometry, Manhattan Poisson line process, Manhattan Poisson line Cox Process, path distance, shortest path.

## I. INTRODUCTION

The study of random spatial patterns, formally called *stochastic geometry*, has played an important role in statistical physics. Some of the well known examples include the study of percolation over both lattices and random sets of points, referred to as *point processes* [1]–[4], as well as the characterization of the properties of tessellations formed by point processes and random sets of lines called *line processes* [5], [6]. In fact, as will be discussed shortly, the modern treatment of line processes was inspired by the study of particle trajectories in a cloud-chamber experiment [7]. The Poisson line process (PLP), which will be defined formally in Section II, is often the preferred choice for analysis in this line of work due to its tractability [8]–[10]. Given its rich history, a lot is already known about the distributional properties of a PLP [11], [12]. However, there has been a growing interest in a doubly stochastic point process that is constructed by defining a random set of points on each line of a PLP in  $\mathbb{R}^2$ , which is relatively less understood and is the focus of this paper. Specifically, we focus on the distribution of the shortest distance between two points of this point process when traveling only along the random lines. This distance, which will henceforth be referred to as the *shortest path distance*, has not been analytically characterized in the literature yet. Before formulating the problem mathematically, it is instructive to discuss the rich history of PLP and the context in which this new doubly stochastic point process has emerged.

As mentioned earlier, the development of the theory of line process was inspired by a problem suggested to S. Goudsmit by N. Bohr, which dealt with the chance of intersection of the trajectories of the sub-atomic particles in a cloud-chamber experiment [7]. This work has motivated a lot of research focused on the various properties of line processes in the latter half of the twentieth century. In particular, R. E. Miles authored a series of papers which explored the fundamental properties of the PLPs and the random polygons generated by the lines of the PLP [12]–[14]. Some of the other prominent works in the literature include the spectral analysis of line processes presented by M. S. Bartlett in [15] and the study of higher order properties of stationary line processes by R. Davidson in [16].

Owing to its analytical tractability, the PLP has found applications in material sciences [17], image processing [18], geology [19], telecommunication [20], [21], and localization networks [22]. In [17], the position of fibers in

V. V. Chetlur and H. S. Dhillon are with Wireless@VT, Department of ECE, Virginia Tech, Blacksburg, VA (email: {vishnu, hdhillon}@vt.edu). C. P. Dettmann is with School of Mathematics, University of Bristol, UK (email: carl.dettmann@bris.ac.uk). The support of the US National Science Foundation (Grant IIS-1633363) and UK Engineering and Physical Sciences Research Council (Grant EP/N002458/1) is gratefully acknowledged.

each layer of a fiber membrane is modeled using PLP to analyze the strength of the membranes. In [20], F. Baccelli proposed to model the road system by a PLP to study the handover behavior in cellular networks. This spatial model was further used by V. Schmidt and his co-authors in the analysis of urban telecommunication networks [21], [23]–[25]. Modeling the obstacles in a cellular assisted localization network by a PLP, the blind spot probability of the typical target node is explored in [22].

A Poisson line Cox process or a Cox process driven by PLP is a doubly stochastic point process constructed by populating points on the lines of a PLP such that the locations of points on each line form a 1D Poisson point process (PPP), which is formally defined in the next section. The PLCP has recently been employed in several works pertaining to the analysis of vehicular communication networks [26]–[30]. Unlike PLPs, the research on PLCPs is still in nascent stages as some of the fundamental properties of the PLCP have only been explored very recently. For instance, the distribution of various Euclidean distances between the points of the PLCP have been derived in [26] to characterize the signal-to-interference plus noise ratio (SINR)-based coverage probability of the typical vehicular node in the network. The Laplace functional of the PLCP is provided in [30] and the asymptotic behavior of the PLCP is studied in [27]. However, these works have only focused on the Euclidean distance properties of the PLCP due to their impact on the network performance.

Although sparse, a few works in the literature have also explored the path distance characteristics of the PLCP. The authors of [21] have analyzed the mean shortest path length between a point of the PLCP and its closest point from another Cox process on the same PLP in the sense of Euclidean distance. The asymptotic behavior of this shortest path distance was investigated in [31]. However, the analytical characterization of the shortest path distance between the typical point and its nearest neighbor in the sense of path distance is still an open problem in the literature and is the main contribution of this paper. For this purpose, we consider a special variant of the PLP called Manhattan Poisson line process (MPLP) which will be discussed in detail in the next section. For a stationary Cox process constructed on the MPLP, referred to as MPLCP, we characterize the length of the shortest path between the typical point of the MPLCP and its nearest neighbor in the sense of the path distance. Specifically, we derive a closed-form analytical expression for the CDF of the shortest path distance for the typical point located at the intersection of two lines. Using this result, we derive remarkably tight bounds for the case where the typical point of the MPLCP is located at some arbitrary position on a line. To the best of our knowledge, this is the first work to present the analytical characterization of path distances in a MPLCP. We also discuss the utility of the path distance characteristics of the MPLCP in providing useful insights in the areas of wireless communications, transportation networks, urban planning, and personnel deployment.

## II. BACKGROUND AND NOTATION

In this section, we present a brief introduction to line processes and some of its fundamental properties. While we discuss only those aspects of line processes that are necessary for this paper, a detailed account of the theory can be found in [11].

### A. Line process preliminaries

As the PPP is a primary building block in the construction of the MPLP considered in our paper, we begin our discussion by defining it formally next.

**Definition 1.** (Poisson point process.) *A random set of points  $\Phi \subset \mathbb{R}^d$  with intensity measure  $\Lambda$  is a PPP if it satisfies the following two properties:*

- *The number of points of  $\Phi$  within any bounded Borel set  $A \subset \mathbb{R}^d$ , denoted by  $\Phi(A)$ , follows a Poisson distribution, i.e.*

$$\mathbb{P}(\Phi(A) = k) = \frac{\exp(-\Lambda(A))(\Lambda(A))^k}{k!}, \quad (1)$$

*where  $\Lambda(A)$  is the average number of points of  $\Phi$  in  $A$ .*

- *The number of points of  $\Phi$  lying in  $n$  disjoint Borel sets form a set of  $n$  independent random variables for arbitrary  $n$ , which is also termed the independent scattering property.*

A PPP is said to be *homogeneous* if it has a constant intensity  $\lambda$ , which is the average number of points per unit volume in  $\mathbb{R}^d$ .

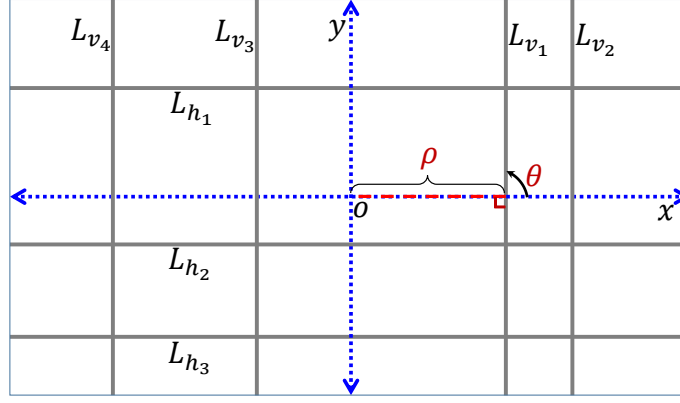


Fig. 1: Illustration of Manhattan Poisson line process in two-dimensional plane  $\mathbb{R}^2$ .

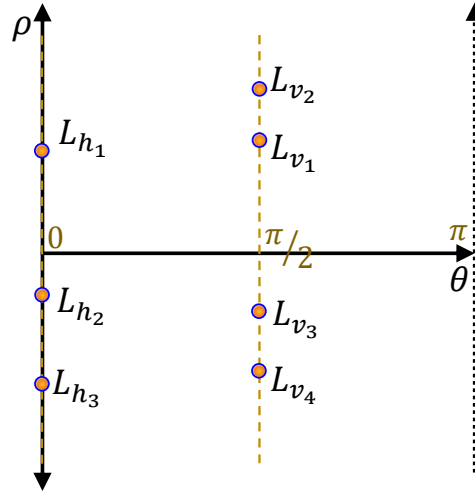


Fig. 2: Illustration of a point process in representation space  $\mathcal{C} \equiv [0, \pi) \times \mathbb{R}$ .

*Line process.* As mentioned in Section I, a line process is just a random collection of lines. In order to define it more formally, first observe that any undirected line  $L$  in  $\mathbb{R}^2$  can be uniquely parameterized by its signed perpendicular distance  $\rho$  from the origin  $o \equiv (0, 0)$  and the angle  $\theta$  subtended by the line with respect to the positive  $x$ -axis in counter clockwise direction, as shown in Fig. 1. The sign of  $\rho$  is negative if the origin is to the right or above the line. Thus, the pair of parameters  $\rho$  and  $\theta$  can be represented as the coordinates of a point on the half-cylinder  $\mathcal{C} \equiv [0, \pi) \times \mathbb{R}$ , which is termed as the *representation space*, as illustrated in Fig. 2. Thus, a random collection of lines in  $\mathbb{R}^2$  can be constructed from a set of points on  $\mathcal{C}$ . Such a set of lines generated by a PPP on  $\mathcal{C}$  is called a PLP.

As mentioned earlier, in this paper, we focus on the special case of PLP called MPLP in which the orientations of the lines are restricted to  $\{0, \pi/2\}$ , thereby obtaining a set of horizontal and vertical lines in  $\mathbb{R}^2$ , as depicted in Fig. 1. Thus, the MPLP  $\Phi_l$  in  $\mathbb{R}^2$  can be constructed from two independent 1D PPPs  $\Psi_0$ , and  $\Psi_{\pi/2}$  along the lines  $\theta = 0$ , and  $\theta = \pi/2$ , respectively, in the representation space  $\mathcal{C}$ . Alternatively, one can construct a MPLP by first populating points along the  $x$  and  $y$ -axes in  $\mathbb{R}^2$  according to independent 1D PPPs  $\Xi_x$  and  $\Xi_y$  and drawing vertical and horizontal lines through those points, respectively. This interpretation is useful in visualizing some of the basic properties of MPLP which will be discussed next. In this paper, we will mainly follow this interpretation for the ease of clarity and exposition.

*Stationarity.* Analogous to a point process, a line process  $\Phi_l$  is stationary if the distribution of lines is invariant to any translation  $T_{(t, \beta)}$ , which corresponds to the translation of the origin by a distance  $t$  in a direction that makes an angle  $\beta$  with respect to positive  $x$ -axis in counter clockwise direction. Upon applying a translation  $T_{(t, \beta)}$ , the representation of a line  $L$  in  $\mathcal{C}$  changes from  $(\rho, \theta)$  to  $(\rho + t \sin(\theta - \beta), \theta)$ . Therefore, a MPLP  $\Phi_l$  is stationary if

the 1D PPPs  $\Psi_0$ , and  $\Psi_{\pi/2}$  are stationary or alternatively,  $\Xi_x$  and  $\Xi_y$  are stationary.

*Line density.* The line density of a line process is defined as the mean line length per unit area. The relationship between the line density and the density of the corresponding point process is given by the following Lemma.

**Lemma 1.** *For a stationary MPLP  $\Phi_l$  constructed from independent and homogeneous 1D PPPs  $\Xi_x$  and  $\Xi_y$ , each with density  $\lambda_l$ , the line density  $\mu_l$  is given by  $\mu_l = 2\lambda_l$ .*

*Proof.* Let us consider a ball of radius  $d$  centered at the origin  $b(o, d)$ . We denote the set of horizontal and vertical lines of  $\Phi_l$  by  $\Phi_{lh}$  and  $\Phi_{lv}$ , respectively. The line density  $\mu_l$  can now be computed as

$$\begin{aligned}
 \mu_l &= \frac{1}{\pi d^2} \mathbb{E} \left[ \sum_{L \in \Phi_l} \nu_1(L \cap b(o, d)) \right] \\
 &= \frac{1}{\pi d^2} \mathbb{E} \left[ \sum_{L_h \in \Phi_{lh}} \nu_1(L_h \cap b(o, d)) + \sum_{L_v \in \Phi_{lv}} \nu_1(L_v \cap b(o, d)) \right] \\
 &= \frac{1}{\pi d^2} \mathbb{E} \left[ \sum_{\substack{\rho_x \in \Xi_x: \\ \rho_x \leq d}} 2\sqrt{d^2 - \rho_x^2} \right] + \frac{1}{\pi d^2} \mathbb{E} \left[ \sum_{\substack{\rho_y \in \Xi_y: \\ \rho_y \leq d}} 2\sqrt{d^2 - \rho_y^2} \right] \\
 &\stackrel{(a)}{=} \frac{1}{\pi d^2} (\lambda_l 2) \left[ \int_0^1 2\sqrt{d^2 - \rho_x^2} d\rho_x + \int_0^1 2\sqrt{d^2 - \rho_y^2} d\rho_y \right] \\
 &= 2\lambda_l,
 \end{aligned}$$

where  $\nu_1(\cdot)$  denotes the one dimensional Lebesgue measure and (a) follows from Campbell's theorem for sums over stationary 1D PPPs  $\Xi_x$  and  $\Xi_y$  [32].  $\square$

*Lines intersecting a region.* For a stationary MPLP  $\Phi_l$  with line density  $\mu_l$ , the number of horizontal and vertical lines that intersect a convex region  $K \subseteq \mathbb{R}^2$  are Poisson distributed with means  $\mu_l \nu_1(K_y)/2$  and  $\mu_l \nu_1(K_x)/2$ , respectively, where  $K_x$  and  $K_y$  denote the projection of  $K$  onto  $x$  and  $y$  axis.

## B. Spatial model and notation

We will now provide a detailed description of the spatial model and also introduce the notation that will be followed in the paper. We consider a stationary MPLP  $\Phi_l \equiv \{L_{h_1}, L_{h_2}, \dots, L_{v_1}, L_{v_2}, \dots\}$  in  $\mathbb{R}^2$  in which the vertical and horizontal lines are generated by independent homogeneous 1D PPPs  $\Xi_x$  and  $\Xi_y$ , each having density  $\lambda_l$ . We denote the set of horizontal and vertical lines by  $\Phi_{lh} \equiv \{L_{h_1}, L_{h_2}, \dots\}$  and  $\Phi_{lv} \equiv \{L_{v_1}, L_{v_2}, \dots\}$ , respectively. We construct a MPLCP  $\Phi_c$  by populating points on the lines of  $\Phi_l$  such that the locations of points on each line form a 1D PPP with density  $\lambda_c$ , as illustrated in Fig. 3. Note that the MPLCP  $\Phi_c$  is also stationary due to the stationarity of the underlying MPLP and the homogeneity of 1D PPP on each line [30], [33]. An arbitrarily chosen point of the MPLCP  $\Phi_c$  is referred to as the typical point. In this paper, we will consider two types of typical points: (i) the typical point located at the intersection of a horizontal and vertical line, and (ii) the typical point located at some arbitrary position on a line.

Without loss of generality, we place the typical point at the origin  $o$  owing to the stationarity of  $\Phi_c$ . Thus, for the case of the typical point located at an intersection, a horizontal line  $L_x$  and a vertical line  $L_y$ , which are aligned along the  $x$  and  $y$ -axes, respectively, pass through the typical point. Therefore, under this conditioning (more formally, under *Palm probability*), the resulting line process is  $\Phi_{l_0, \text{int}} = \Phi_l \cup \{L_x, L_y\}$ , which is a consequence of the Slivnyak's theorem [32], [33]. Thus, under Palm probability, the resulting point process  $\Phi_{c_0, \text{int}}$  can be interpreted as the superposition of the point process  $\Phi_c$ , two 1D PPPs each with density  $\lambda_c$  along the lines  $L_x$  and  $L_y$ , and an atom at the origin [26], [29].

In case of the typical point located at some arbitrary position on a line, without loss of generality, we assume that it is located on a horizontal line of the MPLP  $\Phi_l$ . In this case, upon conditioning on the location of the typical point at the origin and using the same argument as above, the resulting line process is  $\Phi_{l_0, \text{gen}} = \Phi_l \cup \{L_x\}$ . Thus, the resulting point process  $\Phi_{c_0, \text{gen}}$  can be interpreted as the superposition of the point process  $\Phi_c$ , an independent 1D PPP with density  $\lambda_c$  on the line  $L_x$  aligned along the  $x$ -axis and an atom at the origin. Our main goal is to

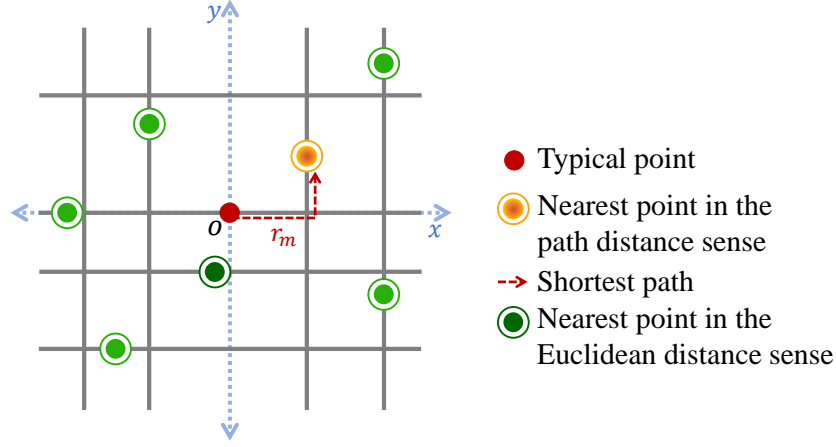


Fig. 3: Illustration of the spatial model.

characterize the length of the shortest path from the location of the typical point to its nearest neighbor in the sense of path distance for both the cases. We formally define the path distance between two points as follows.

**Definition 2.** (Path distance.) *The path distance between two points  $\mathbf{a}(x_1, y_1)$  and  $\mathbf{b}(x_2, y_2)$  is defined as the sum of lengths of the line segments that constitute a path  $P$  from  $\mathbf{a}$  to  $\mathbf{b}$  and is denoted by  $\ell(\mathbf{a}, \mathbf{b})$ .*

We denote the number of horizontal and vertical lines that intersect a region  $A \subset \mathbb{R}^2$  by  $N_h(A)$  and  $N_v(A)$ , respectively. We denote the number of points of the MPLCP located in the set  $A$  by  $N_p(A)$ . In this paper, we will denote the random variables by upper case letters and their corresponding realizations by lower case letters. For example,  $W$  denotes a random variable, whereas  $w$  denotes its realization. We defer the definition of other variables to later sections of the paper for better readability.

### III. ANALYTICAL RESULTS

In this section, we will characterize the distribution of the shortest path distance  $R_m$ . First, we will determine the exact CDF of  $R_m$  for the typical point located at the intersection. Building on this result, we will provide an upper bound and an approximate lower bound for the CDF of  $R_m$  for the case where the typical point is located at some arbitrary position.

#### A. Typical point at intersection

In this case, for the typical point located at the origin, the length of the shortest path to any point located at  $(x_i, y_i)$  is simply given by  $z_i = |x_i| + |y_i|$ , which is nothing but the first order Minkowski distance of the point from the origin. If the closest point to the typical point (in the sense of path distance) is at a distance  $r_m$ , then there can not be any point at a location  $(x, y)$  in  $\mathbb{R}^2$  such that  $|x| + |y| < r_m$ . Thus, as depicted in Fig. 4, we obtain an exclusion zone  $B_0$  formed by the intersection of the half-planes  $x + y < r_m$ ,  $-x + y < r_m$ ,  $-x - y < r_m$ , and  $x - y < r_m$ . There can be no points on any of the line segments inside the square region  $B_0$ . In addition to  $L_x$  and  $L_y$ , we know that there are a random number of lines that intersect the region  $B_0$ . From the construction of MPLP, it follows that the number of horizontal and vertical lines that intersect  $B_0$  are Poisson distributed with mean  $\lambda_l 2r_m$ . For a horizontal line located at a distance  $y_l < r_m$  from the origin, the length of the line segment inside  $B_0$  is given by  $2r_m - 2y_l$ . Similarly, for a vertical line at a distance  $x_l < r_m$  from the origin, the length of the line segment inside  $B_0$  is  $2r_m - 2x_l$ . Using these properties, we will now derive a closed-form expression for the CDF of the shortest path distance  $R_m$  in the following theorem.

**Theorem 1.** *The CDF of the shortest path distance from the typical point located at an intersection to its nearest neighbor in the sense of path distance is*

$$F_{R_m}(r_m) = 1 - \exp \left[ -4\lambda_c r_m - 4\lambda_l r_m + \frac{2\lambda_l}{\lambda_c} \left( 1 - e^{-2\lambda_c r_m} \right) \right]. \quad (2)$$

*Proof.* The CDF of  $R_m$  can be computed as

$$\begin{aligned}
F_{R_m}(r_m) &= 1 - \mathbb{P}(R_m > r_m) \\
&= 1 - \mathbb{P}(N_p(\Phi_{l_0, \text{int}} \cap B_0) = 0) \\
&\stackrel{(a)}{=} 1 - \mathbb{P}\left(N_p(\{L_x \cup \Phi_{lh}\} \cap B_0) = 0\right) \mathbb{P}\left(N_p(\{L_y \cup \Phi_{lv}\} \cap B_0) = 0\right) \\
&\stackrel{(b)}{=} 1 - \left[ \mathbb{P}(N_p(L_x \cap B_0) = 0) \sum_{n_{hl}=0}^{\infty} \mathbb{P}(N_h(B_0 \setminus L_x) = n_{hl}) \right. \\
&\quad \times \mathbb{P}\left(N_p(\Phi_{lh} \cap B_0) = 0 | N_h(B_0 \setminus L_x) = n_{hl}\right) \left. \right] \left[ \mathbb{P}(N_p(L_y \cap B_0) = 0) \right. \\
&\quad \times \sum_{n_{vl}=0}^{\infty} \mathbb{P}(N_v(B_0 \setminus L_y) = n_{vl}) \mathbb{P}\left(N_p(\Phi_{lv} \cap B_0) = 0 | N_v(B_0 \setminus L_y) = n_{vl}\right) \left. \right] \\
&\stackrel{(c)}{=} 1 - \left[ \mathbb{P}(N_p(L_x \cap B_0) = 0) \sum_{n_{hl}=0}^{\infty} \mathbb{P}(N_h(B_0 \setminus L_x) = n_{hl}) \right. \\
&\quad \times \left( \prod_{j=1}^{n_{hl}} \mathbb{P}(N_p(L_{h_j} \cap B_0) = 0) \right) \left. \right] \left[ \mathbb{P}(N_p(L_y \cap B_0) = 0) \right. \\
&\quad \times \sum_{n_{vl}=0}^{\infty} \mathbb{P}(N_v(B_0 \setminus L_y) = n_{vl}) \left( \prod_{k=1}^{n_{vl}} \mathbb{P}(N_p(L_{v_k} \cap B_0) = 0) \right) \left. \right] \\
&\stackrel{(d)}{=} 1 - \left[ e^{-2\lambda_c r_m} \sum_{n_{hl}=0}^{\infty} \frac{e^{-2\lambda_l r_m} (2\lambda_l r_m)^{n_{hl}}}{n_{hl}!} \left( \int_0^{r_m} \exp(-\lambda_c(2r_m - 2y)) \frac{dy}{r_m} \right)^{n_{hl}} \right] \\
&\quad \times \left[ e^{-2\lambda_c r_m} \sum_{n_{vl}=0}^{\infty} \frac{e^{-2\lambda_l r_m} (2\lambda_l r_m)^{n_{vl}}}{n_{vl}!} \left( \int_0^{r_m} \exp(-\lambda_c(2r_m - 2x)) \frac{dx}{r_m} \right)^{n_{vl}} \right] \\
&= 1 - \left[ e^{-2\lambda_c r_m} e^{-2\lambda_l r_m} \exp \left[ 2\lambda_l \int_0^{r_m} e^{-2\lambda_c(r_m - y)} dy \right] \right] \\
&\quad \times \left[ e^{-2\lambda_c r_m} e^{-2\lambda_l r_m} \exp \left[ 2\lambda_l \int_0^{r_m} e^{-2\lambda_c(r_m - x)} dx \right] \right] \\
&= 1 - \exp \left[ -4\lambda_c r_m - 4\lambda_l r_m + \frac{2\lambda_l}{\lambda_c} (1 - e^{-2\lambda_c r_m}) \right],
\end{aligned}$$

where (a) follows from the fact that the distribution of horizontal and vertical lines are independent, (b) follows from conditioning on the number of horizontal and vertical lines intersecting the region  $B_0$ , (c) follows from the independent distribution of points on the lines, and (d) follows from the Poisson distribution of the number of lines intersecting  $B_0$  and the void probability of 1D PPP on each line.  $\square$

### B. Typical point at arbitrary position

In this subsection, we derive an upper bound and an approximate lower bound for the CDF of  $R_m$  for the typical point located at the origin on the horizontal line  $L_x$  aligned along the  $x$ -axis.

**Remark 1.** The key difference between the spatial setup in this case and the previous case is that there does not exist a line  $L_y$  along the  $y$ -axis in this setup. More precisely, the point process is now viewed under the reduced Palm distribution of  $\Xi_x$  and Palm distribution of  $\Xi_y$ . This interpretation will allow us to derive an upper bound for the distribution of  $R_m$  for the typical point using the results derived in Theorem 1.

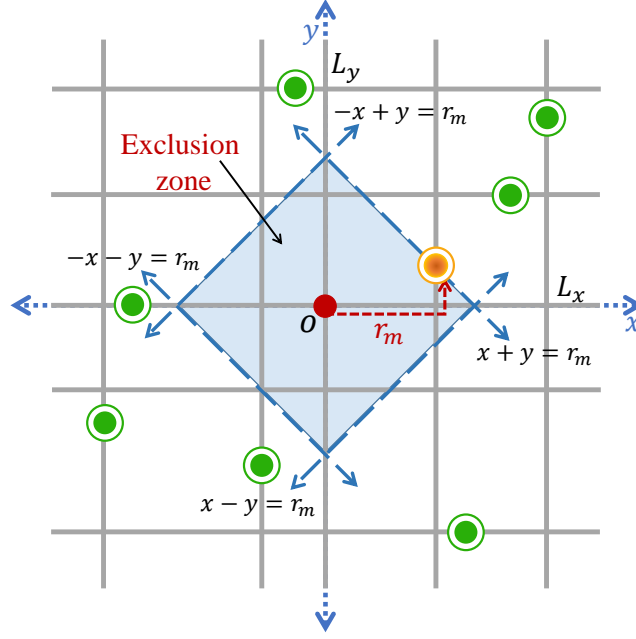


Fig. 4: Illustration of the exclusion zone for the typical point located at an intersection.

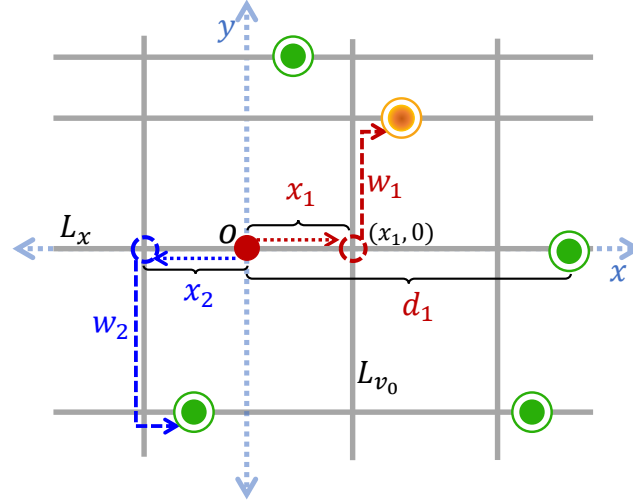


Fig. 5: Illustration of the shortest paths for the typical point located at arbitrary position on the line  $L_x$ .

1) *Upper bound:* As mentioned in Remark 1, there is no vertical line at the origin for the typical point located at some arbitrary position on  $L_x$ . Consequently, the paths starting from the typical point are only along the direction of either positive or negative  $x$ -axis on the line  $L_x$ , whereas the paths for the typical point at the intersection start in any of the four directions from the origin. Therefore, unlike the previous case, where the length of the shortest path to any point was equal to the first order Minkowski distance, the distance to some points from the origin in this case is greater than their first order Minkowski distance, as illustrated in Fig. 5. Thus, in this case, the first order Minkowski distance of the nearest point from the origin is a lower bound on  $R_m$ . Therefore, using the result derived in Theorem 1, we present a closed-form upper bound on the CDF of  $R_m$  in the following proposition.

**Proposition 1.** *For the typical point located at some arbitrary position on the line  $L_x$ , the CDF of the shortest path distance  $R_m$  to the nearest neighbor in the sense of path distance is upper bounded by*

$$F_{R_m}(r_m) \leq 1 - \exp \left[ -2\lambda_c r_m - 4\lambda_l r_m + \frac{2\lambda_l}{\lambda_c} \left( 1 - e^{-2\lambda_c r_m} \right) \right]. \quad (3)$$

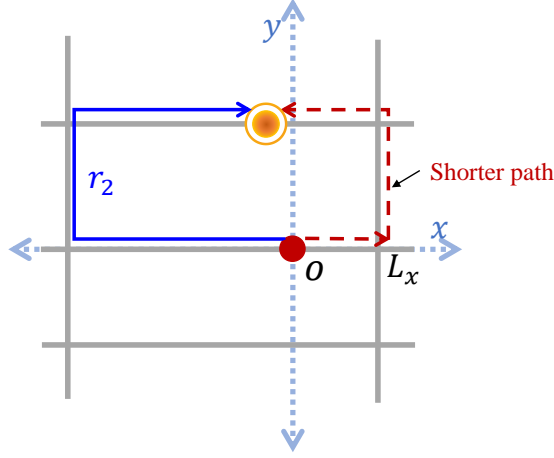


Fig. 6: Illustration of the scenario in which the shortest path to a point to the left of the  $y$ -axis is the one that starts in the direction of positive  $x$ -axis.

*Proof.* This result can be directly derived from the expression in Theorem 1 by deleting the line  $L_y$ . This means that we remove the terms corresponding to the vertical line  $L_y$  aligned along the  $y$ -axis. Specifically, we remove the term  $\mathbb{P}(N_p(L_y \cap B_0) = 0)$  in step (a) and the corresponding expressions in the subsequent steps in the proof of Theorem 1 to obtain the final expression.  $\square$

As will be shown in the next section, this upper bound is reasonable but not extremely tight. We will derive a much tighter lower bound for the CDF of  $R_m$  next.

2) *Approximate lower bound:* We define a random variable  $R_1$  as the shortest path distance from the origin to the nearest point of  $\Phi_c$  located to the right of  $y$ -axis upon starting in the direction of positive  $x$ -axis. Similarly, we define  $R_2$  as the shortest path distance to the nearest point located to the left of the  $y$ -axis when starting in the direction of negative  $x$ -axis. Thus, the overall shortest path distance to a point from the origin can be written as  $R_m \leq \min\{R_i\}_{i=1,2}$ . The inequality is due to the fact that for some points to the right and left of  $y$ -axis, the shortest path from the origin would be the one that starts along the direction of negative and positive  $x$ -axis from the origin, respectively, as illustrated in Fig. 6. So, in such scenarios,  $R_1$  or  $R_2$  would be an upper bound on the shortest path distances to those points. Therefore, the CDF of  $R_m$  would be bounded from below by the CDF of  $\min\{R_i\}_{i=1,2}$ .

For the paths starting in any of the two directions from the origin, there are two possibilities: (i) the path to the nearest point must cross at least one intersection, and (ii) the nearest point is on the same line  $L_x$  before any intersection. Therefore,  $R_i$  can be mathematically written as

$$R_i = \begin{cases} X_i + W_i, & \mathcal{E}_{0,i} \text{ occurs,} \\ D_i, & \mathcal{E}_{1,i} \text{ occurs.} \end{cases} \quad (4)$$

We now define all the random variables appearing in (4). For notational consistency, we use the subscript  $i = 1$  to denote the variables corresponding to the path starting in the positive  $x$ -axis direction and the subscript  $i = 2$  for the path starting in the negative  $x$ -direction. The event in which the shortest path to the nearest point contains an intersection is denoted by  $\mathcal{E}_{0,i}$  and its complementary event is denoted by  $\mathcal{E}_{1,i}$ .  $D_i$  denotes the distance to the closest point from the origin and  $X_i$  denotes the distance to the first intersection from the origin in the direction of the path, as shown in Fig. 5.  $W_1$  and  $W_2$  denote the shortest first order Minkowski distance from the intersection to the points located to the right and left of the  $y$ -axis, respectively.

As the locations of points on each line follows a 1D PPP with mean  $\lambda_c$ , the distance  $D_i$  is exponentially distributed with mean  $\lambda_c^{-1}$ . Thus, the CDF and PDF of  $D_i$  are

$$\text{CDF: } F_{D_i}(d_i) = 1 - \exp(-\lambda_c d_i), \quad (5)$$

$$\text{PDF: } f_{D_i}(d_i) = \lambda_c \exp(-\lambda_c d_i). \quad (6)$$



Since the points at which the vertical lines cross the  $x$ -axis form a 1D PPP with density  $\lambda_l$ , the distance  $X_i$  also follows an exponential distribution with mean  $\lambda_l^{-1}$ . Thus, the CDF and PDF of  $X_i$  are

$$\text{PDF: } f_{X_i}(x_i) = \lambda_l \exp(-\lambda_l x_i). \quad (8)$$

**Lemma 2.** *The probability of occurrence of the events  $\mathcal{E}_{0,1}$  and  $\mathcal{E}_{1,1}$  are given by*

*Proof.* The probability of the event  $\mathcal{E}_{0,1}$  can be calculated as

Since the events  $\mathcal{E}_{0,1}$  and  $\mathcal{E}_{1,1}$  are complementary, the probability of occurrence of  $\mathcal{E}_{1,1}$  can be calculated as  $\mathbb{P}(\mathcal{E}_{1,1}) = 1 - \mathbb{P}(\mathcal{E}_{0,1})$ . This completes the proof.  $\square$

We will focus on the computation of the CDF of  $W_1$  conditioned on the event  $\mathcal{E}_{0,1}$  next. The conditioning on  $\mathcal{E}_{0,1}$  implies that there does not exist any point between the origin and the intersection. This additional information about the distribution of points in the interval  $[0, X_1]$  on  $L_x$  must be included in the computation of the conditional CDF of  $W_1$ . Since the distance  $X_1$  is random, we will derive the intermediate results by additionally conditioning on  $X_1$  and we will take expectation over  $X_1$  in the final step in the computation of the marginal CDF of  $R_1$ . Similar to the procedure followed in the derivation of Theorem 1, we will consider an exclusion zone  $B$  formed by the intersection of the half-planes  $(x - x_1) + y < w_1$ ,  $-(x - x_1) + y < w_1$ ,  $-(x - x_1) - y < w_1$ ,  $(x - x_1) - y < w_1$ ,

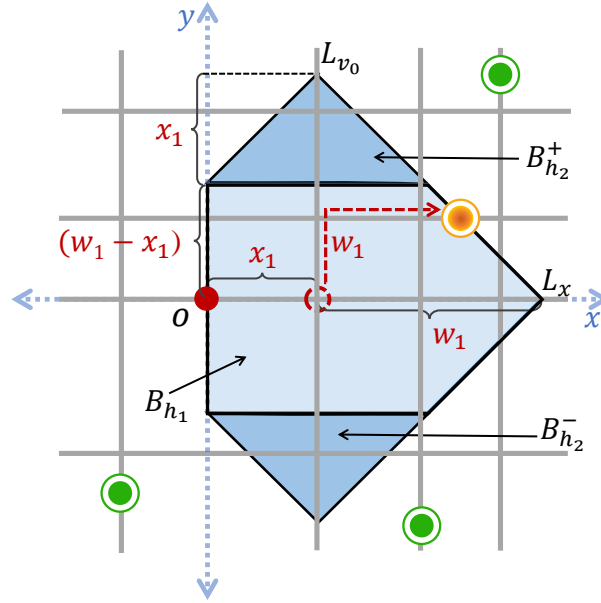


Fig. 8: Illustration of the exclusion zone for the case  $w_1 \geq x_1$ .

and  $x > 0$ . Note that the shape of the exclusion region  $B$  depends on the values of  $w_1$  with respect to  $x_1$ . While  $B$  is a square for  $w_1 < x_1$ , it is a pentagon for  $w_1 \geq x_1$ , as shown in Figs. 7 and 8, respectively. So, we will derive the conditional CDF of  $W_1$  for the two cases  $w_1 < x_1$  and  $w_1 \geq x_1$  separately. We know that there can not be any point on any of the line segments inside  $B$ . In addition to  $L_x$ , there exists a random number of horizontal lines above and below the line  $L_x$  that intersect the region  $B$ . Likewise, in addition to the vertical line of the intersection  $L_{v_0}$ , there exists a random number of vertical lines that intersect the region  $B$ . However, conditioned on the event  $\mathcal{E}_{0,1}$ , the distribution of vertical lines to the left of  $L_{v_0}$  is not the same as the distribution of lines to the right of  $L_{v_0}$ . Since the first intersection to the right of the origin is at a distance  $x_1$ , there can not be any vertical line that intersects  $L_x$  in the interval  $[0, x_1)$ , as shown in Fig. 7. So, we just need to focus on the set of vertical lines that intersect the region  $B_{x_1^+} = B \cap \{x > x_1\}$ . We will now derive a closed form expression for the conditional CDF of  $W_1$  in the following Lemma.

**Lemma 3.** *The CDF of  $W_1$  conditioned on  $\mathcal{E}_{0,1}$  and  $X_1$  is given by*

$$F_{W_1}(w_1|\mathcal{E}_{0,1}, x_1) = \begin{cases} F_{W_1,1}(w_1|\mathcal{E}_{0,1}, x_1), & 0 \leq w_1 < x_1, \\ F_{W_1,2}(w_1|\mathcal{E}_{0,1}, x_1), & w_1 \geq x_1, \end{cases} \quad (10)$$

where

$$F_{W_1,1}(w_1|\mathcal{E}_{0,1}, x_1) = 1 - \exp \left[ -3\lambda_c w_1 - 3\lambda_l w_1 + \frac{3\lambda_l}{2\lambda_c} (1 - e^{-2\lambda_c w_1}) \right],$$

and

$$F_{W_1,2}(w_1|\mathcal{E}_{0,1}, x_1) = 1 - \exp \left[ -3(\lambda_c + \lambda_l)w_1 - \lambda_c x_1 + \frac{\lambda_l}{2\lambda_c} (3 + 2e^{-2\lambda_c x_1} - e^{-2\lambda_c w_1} - 4e^{-\lambda_c(x_1+w_1)}) \right]. \quad (11)$$

*Proof.* The conditional CDF of  $W_1$  can be computed as

$$\begin{aligned} F_{W_1}(w_1|\mathcal{E}_{0,1}, x_1) &= 1 - \mathbb{P}(W_1 > w_1|\mathcal{E}_{0,1}, X_1) \\ &= 1 - \mathbb{P}(N_p(B) = 0|\mathcal{E}_{0,1}, X_1). \end{aligned} \quad (12)$$

As we had discussed earlier, the shape of the exclusion zone  $B$  is different for the two cases  $w_1 < x_1$  and  $w_1 \geq x_1$  and hence we will handle these two cases separately. We will first consider the case  $w_1 < x_1$ . In this case,  $B$  is a square region and we now need to determine the probability that there are no points inside this square region centered at an intersection, as shown in Fig. 7. By expressing the conditional void probability in (12) as the product of void probabilities of independent individual components, as in the proof of Theorem 1, we obtain

$$\begin{aligned}
& \mathbb{P}(N_p(B) = 0 | \mathcal{E}_{0,1}, X_1) \\
&= \mathbb{P}(N_p(L_x \cap B) = 0 | \mathcal{E}_{0,1}, X_1) \left[ \sum_{n_{hl}=0}^{\infty} \mathbb{P}(N_h(B \setminus L_x) = n_{hl} | \mathcal{E}_{0,1}, X_1) \right. \\
&\quad \times \mathbb{P}(N_p(\Phi_{lh} \cap B) = 0 | N_h(B \setminus L_x) = n_{hl}, \mathcal{E}_{0,1}, X_1) \left. \right] \\
&\quad \times \mathbb{P}(N_p(L_{v_0} \cap B) = 0 | \mathcal{E}_{0,1}, X_1) \left[ \sum_{n_{vl}=0}^{\infty} \mathbb{P}(N_v(B_{x_1^+}) = n_{vl} | \mathcal{E}_{0,1}, X_1) \right. \\
&\quad \times \mathbb{P}(N_p(\Phi_{lv} \cap B_{x_1^+}) = 0 | N_v(B_{x_1^+}) = n_{vl}, \mathcal{E}_{0,1}, X_1) \left. \right] \\
&\stackrel{(a)}{=} \mathbb{P}(N_p(L_x \cap B) = 0 | \mathcal{E}_{0,1}, X_1) \left[ \sum_{n_{hl}=0}^{\infty} \mathbb{P}(N_h(B \setminus L_x) = n_{hl}) \right. \\
&\quad \times \mathbb{P}(N_p(\Phi_{lh} \cap B) = 0 | N_h(B \setminus L_x) = n_{hl}) \left. \right] \\
&\quad \times \mathbb{P}(N_p(L_{v_0} \cap B) = 0) \left[ \sum_{n_{vl}=0}^{\infty} \mathbb{P}(N_v(B_{x_1^+}) = n_{vl}) \right. \\
&\quad \times \mathbb{P}(N_p(\Phi_{lv} \cap B_{x_1^+}) = 0 | N_v(B_{x_1^+}) = n_{vl}) \left. \right] \\
&\stackrel{(b)}{=} \mathbb{P}(N_p(L_x \cap B) = 0 | \mathcal{E}_{0,1}, X_1) \left[ \sum_{n_{hl}=0}^{\infty} \mathbb{P}(N_h(B \setminus L_x) = n_{hl}) \right. \\
&\quad \times \left( \prod_{j=1}^{n_{hl}} \mathbb{P}(N_p(L_{h_j} \cap B) = 0) \right) \left. \right] \mathbb{P}(N_p(L_{v_0} \cap B) = 0) \\
&\quad \times \left[ \sum_{n_{vl}=0}^{\infty} \mathbb{P}(N_v(B_{x_1^+}) = n_{vl}) \left( \prod_{k=1}^{n_{vl}} \mathbb{P}(N_p(L_{v_k} \cap B_{x_1^+}) = 0) \right) \right] \\
&\stackrel{(c)}{=} e^{-\lambda_c w_1} \left[ \sum_{n_{hl}=0}^{\infty} \frac{e^{-2\lambda_l w_1} (2\lambda_l w_1)^{n_{hl}}}{n_{hl}!} \right. \\
&\quad \times \left( \int_0^{w_1} \exp(-\lambda_c(2w_1 - 2y)) \frac{dy}{w_1} \right)^{n_{hl}} \left. \right] e^{-2\lambda_c w_1} \\
&\quad \times \left[ \sum_{n_{vl}=0}^{\infty} \frac{e^{-\lambda_l w_1} (\lambda_l w_1)^{n_{vl}}}{n_{vl}!} \left( \int_0^{w_1} \exp(-\lambda_c(2w_1 - 2x)) \frac{dx}{w_1} \right)^{n_{vl}} \right] \\
&= \left[ e^{-\lambda_c w_1} e^{-2\lambda_l w_1} \exp \left[ 2\lambda_l \int_0^{w_1} e^{-2\lambda_c(w_1 - y)} dy \right] \right] \\
&\quad \times \left[ e^{-2\lambda_c w_1} e^{-\lambda_l w_1} \exp \left[ \lambda_l \int_0^{w_1} e^{-2\lambda_c(w_1 - x)} dx \right] \right] \\
&= \exp \left[ -3\lambda_c w_1 - 3\lambda_l w_1 + \frac{3\lambda_l}{2\lambda_c} (1 - e^{-2\lambda_c w_1}) \right], \tag{13}
\end{aligned}$$

where (a) follows from the fact that the distribution of points on the random horizontal lines, random vertical lines

intersecting  $B_{x_1^+}$ , and the line  $L_{v_0}$  is independent of  $\mathcal{E}_{0,1}$  and  $X_1$ , (b) follows from the independent distribution of points over different lines, and (c) follows from the Poisson distribution of lines and the void probability of 1D PPPs on those lines. Substituting (13) in (12), we obtain the expression for the conditional CDF of  $W_1$  for the case  $w_1 < x_1$ .

We will now consider the case where  $w_1 \geq x_1$ , where the exclusion region  $B$  is a pentagon as depicted in Fig. 8. The length of the horizontal line segment inside  $B$  depends on the distance of the line from the origin. For a horizontal line  $L_h$  which intercepts the  $y$ -axis at  $y_h$  such that  $|y_h| < w_1 - x_1$ , the length of the line segment inside  $B$  is given by  $x_1 + w_1 - |y_h|$ . On the other hand, if  $|y_h| \geq w_1 - x_1$ , then the length of line segment inside  $B$  is  $2(w_1 - |y_h|)$ . So, we partition the set of horizontal lines that intersect  $B$  into two sets: (i) the set of horizontal lines that intersect the region  $B_{h_1} = B \cap \{|y| < w_1 - x_1\}$ , and (ii) the set of horizontal lines that intersect the region  $B_{h_2} = B \cap \{|y| \geq w_1 - x_1\}$ . As  $B_{h_2}$  is composed of two non-contiguous regions  $B_{h_2}^+ = B \cap \{y \geq w_1 - x_1\}$  and  $B_{h_2}^- = B \cap \{y \leq -(w_1 - x_1)\}$ , we will handle them separately in our analysis. Thus, the conditional void probability for the case  $w_1 \geq x_1$  can be computed as

$$\begin{aligned}
& \mathbb{P}(N_p(B) = 0 | \mathcal{E}_{0,1}, X_1) \\
&= \mathbb{P}(N_p(L_x \cap B) = 0 | \mathcal{E}_{0,1}, X_1) \left[ \sum_{n_{h_1}=0}^{\infty} \mathbb{P}(N_h(B_{h_1} \setminus L_x) = n_{h_1} | \mathcal{E}_{0,1}, X_1) \right. \\
&\quad \times \mathbb{P}(N_p(\Phi_{lh} \cap B_{h_1}) = 0 | N_h(B_{h_1} \setminus L_x) = n_{h_1}, \mathcal{E}_{0,1}, X_1) \left. \right] \\
&\quad \times \left[ \sum_{n_{h_2}=0}^{\infty} \mathbb{P}(N_h(B_{h_2}^+) = n_{h_2} | \mathcal{E}_{0,1}, X_1) \mathbb{P}(N_p(\Phi_{lh} \cap B_{h_2}^+) = 0 | N_h(B_{h_2}^+) = n_{h_2}, \mathcal{E}_{0,1}, X_1) \right. \\
&\quad \times \sum_{n_{h_3}=0}^{\infty} \mathbb{P}(N_h(B_{h_2}^-) = n_{h_3} | \mathcal{E}_{0,1}, X_1) \mathbb{P}(N_p(\Phi_{lh} \cap B_{h_2}^-) = 0 | N_h(B_{h_2}^-) = n_{h_3}, \mathcal{E}_{0,1}, X_1) \left. \right] \\
&\quad \times \mathbb{P}(N_p(L_{v_0} \cap B) = 0 | \mathcal{E}_{0,1}, X_1) \left[ \sum_{n_{v_1}=0}^{\infty} \mathbb{P}(N_v(B_{x_1^+}) = n_{v_1} | \mathcal{E}_{0,1}, X_1) \right. \\
&\quad \times \mathbb{P}(N_p(\Phi_{lv} \cap B_{x_1^+}) = 0 | N_v(B_{x_1^+}) = n_{v_1}, \mathcal{E}_{0,1}, X_1) \left. \right] \\
&\stackrel{(a)}{=} \mathbb{P}(N_p(L_x \cap B) = 0 | \mathcal{E}_{0,1}, X_1) \mathbb{P}(N_p(L_{v_0} \cap B) = 0) \left[ \sum_{n_{h_1}=0}^{\infty} \mathbb{P}(N_h(B_{h_1} \setminus L_x) = n_{h_1} | X_1) \right. \\
&\quad \times \mathbb{P}(N_p(\Phi_{lh} \cap B_{h_1}) = 0 | N_h(B_{h_1} \setminus L_x) = n_{h_1}, X_1) \left. \right] \left[ \sum_{n_{h_2}=0}^{\infty} \mathbb{P}(N_h(B_{h_2}^+) = n_{h_2} | X_1) \right. \\
&\quad \times \mathbb{P}(N_p(\Phi_{lh} \cap B_{h_2}^+) = 0 | N_h(B_{h_2}^+) = n_{h_2}, X_1) \sum_{n_{h_3}=0}^{\infty} \mathbb{P}(N_h(B_{h_2}^-) = n_{h_3} | X_1) \\
&\quad \times \mathbb{P}(N_p(\Phi_{lh} \cap B_{h_2}^-) = 0 | N_h(B_{h_2}^-) = n_{h_3}, X_1) \left. \right] \left[ \sum_{n_{v_1}=0}^{\infty} \mathbb{P}(N_v(B_{x_1^+}) = n_{v_1} | X_1) \right. \\
&\quad \times \mathbb{P}(N_p(\Phi_{lv} \cap B_{x_1^+}) = 0 | N_v(B_{x_1^+}) = n_{v_1}, X_1) \left. \right], \\
&\stackrel{(b)}{=} \mathbb{P}(N_p(L_x \cap B) = 0 | \mathcal{E}_{0,1}, X_1) \mathbb{P}(N_p(L_{v_0} \cap B) = 0) \\
&\quad \times \left[ \sum_{n_{h_1}=0}^{\infty} \mathbb{P}(N_h(B_{h_1} \setminus L_x) = n_{h_1} | X_1) \left( \prod_{i=1}^{n_{h_1}} \mathbb{P}(N_p(L_{h_i} \cap B_{h_1}) = 0 | X_1) \right) \right] \\
&\quad \times \left[ \sum_{n_{h_2}=0}^{\infty} \mathbb{P}(N_h(B_{h_2}^+) = n_{h_2} | X_1) \left( \prod_{j=1}^{n_{h_2}} \mathbb{P}(N_p(L_{h_j} \cap B_{h_2}^+) = 0 | X_1) \right) \right]
\end{aligned}$$

$$\begin{aligned}
& \times \sum_{n_{h_3}=0}^{\infty} \mathbb{P}(N_h(B_{h_2}^-) = n_{h_3} | X_1) \left( \prod_{j=1}^{n_{h_3}} \mathbb{P}(N_p(L_{h_j} \cap B_{h_2}^-) = 0 | X_1) \right) \Big] \\
& \times \sum_{n_{vl}=0}^{\infty} \mathbb{P}(N_v(B_{x_1}^+) = n_{vl}) \left( \prod_{k=1}^{n_{vl}} \mathbb{P}(N_p(L_{v_k} \cap B_{x_1}^+) = 0) \right) \Big] \\
& \stackrel{(c)}{=} e^{-\lambda_c(w_1+x_1)} e^{-2\lambda_c w_1} \\
& \times \left[ \sum_{n_{h_1}=0}^{\infty} \frac{e^{-2\lambda_l(w_1-x_1)} (2\lambda_l(w_1-x_1))^{n_{h_1}}}{n_{h_1}!} \left( \int_0^{w_1-x_1} \exp(-\lambda_c(x_1+w_1-y)) \frac{dy}{(w_1-x_1)} \right)^{n_{h_1}} \right] \\
& \times \left[ \sum_{n_{h_2}=0}^{\infty} \frac{e^{-\lambda_l x_1} (\lambda_l x_1)^{n_{h_2}}}{n_{h_2}!} \left( \int_{w_1-x_1}^{w_1} e^{-\lambda_c(2w_1-2y)} \frac{dy}{x_1} \right)^{n_{h_2}} \sum_{n_{h_3}=0}^{\infty} \frac{e^{-\lambda_l x_1} (\lambda_l x_1)^{n_{h_3}}}{n_{h_3}!} \right. \\
& \times \left. \left( \int_{w_1-x_1}^{w_1} e^{-\lambda_c(2w_1-2y)} \frac{dy}{x_1} \right)^{n_{h_3}} \right] \left[ \sum_{n_{vl}=0}^{\infty} \frac{e^{-\lambda_l w_1} (\lambda_l w_1)^{n_{vl}}}{n_{vl}!} \left( \int_0^{w_1} e^{-\lambda_c(2w_1-2x)} \frac{dx}{w_1} \right)^{n_{vl}} \right] \\
& = \exp \left[ -3(\lambda_c + \lambda_l)w_1 - \lambda_c x_1 + \frac{\lambda_l}{2\lambda_c} (3 + 2e^{-2\lambda_c x_1} - e^{-2\lambda_c w_1} - 4e^{-\lambda_c(x_1+w_1)}) \right], \tag{14}
\end{aligned}$$

where (a) follows from the fact that the distribution of points on the random horizontal lines, vertical lines intersecting  $B_{x_1}^+$  and the line  $L_{v_0}$  are independent of  $\mathcal{E}_{0,1}$ , (b) follows from the independent distribution of points over lines, and (c) follows from the Poisson distribution of lines and the void probability of 1D PPPs on each of those lines. Substituting (14) in (12), we obtain the expression for the conditional CDF of  $W_1$  for the case  $w_1 \geq x_1$ . This completes the proof.  $\square$

Having determined all the components required to compute the CDF of  $R_1$  conditioned on  $\mathcal{E}_{0,1}$ , we will now proceed to the derivation of CDF of  $R_1$  conditioned on  $\mathcal{E}_{1,1}$  in the following Lemma.

**Lemma 4.** *Conditioned on the event  $\mathcal{E}_{1,1}$ , the CDF of  $R_1$  is given by*

$$F_{R_1}(r_1 | \mathcal{E}_{1,1}) = 1 - \exp(-(\lambda_l + \lambda_c)r_1). \tag{15}$$

*Proof.* The conditional CDF of  $R_1$  can be computed as

$$\begin{aligned}
F_{R_1}(r_1 | \mathcal{E}_{1,1}) &= \mathbb{P}(R_1 < r_1 | \mathcal{E}_{1,1}) \\
&= 1 - \frac{\mathbb{P}(R_1 > r_1, \mathcal{E}_{1,1})}{\mathbb{P}(\mathcal{E}_{1,1})} \\
&\stackrel{(a)}{=} 1 - \frac{\mathbb{P}(D_1 > r_1, D_1 < X_1)}{\mathbb{P}(\mathcal{E}_{1,1})} \\
&= 1 - \frac{1}{\mathbb{P}(\mathcal{E}_{1,1})} \mathbb{E}_{X_1} [\mathbb{P}(r_1 < D_1 < X_1 | X_1)] \\
&= 1 - \frac{1}{\mathbb{P}(\mathcal{E}_{1,1})} \int_{r_1}^{\infty} (F_{D_1}(x_1) - F_{D_1}(r_1)) f_{X_1}(x_1) dx_1 \\
&= 1 - \frac{\lambda_l + \lambda_c}{\lambda_c} \int_{r_1}^{\infty} (e^{-\lambda_c r_1} - e^{-\lambda_c x_1}) \lambda_l e^{-\lambda_l x_1} dx_1 \\
&= 1 - \exp(-(\lambda_l + \lambda_c)r_1),
\end{aligned}$$

where (a) follows from the condition for the occurrence of the event  $\mathcal{E}_{1,1}$ .  $\square$

With this, we have derived all the intermediate results required to compute the CDF of  $R_1$ . Combining these results given in Lemmas 2, 3, and 4, we will now derive the marginal CDF of  $R_1$  in the following Lemma.

**Lemma 5.** *The CDF of  $R_1$  is*

$$F_{R_1}(r_1) = \int_{\frac{r_1}{2}}^{r_1} F_{W_1,1}(r_1 - x_1 | \mathcal{E}_{0,1}, x_1) \mathbb{P}(\mathcal{E}_{0,1} | X_1) f_{X_1}(x_1) dx_1$$

$\lambda_l \backslash \lambda_c$	10	15	20	25
5	.0669	.0422	.0108	.0056
10	.0095	.0076	.0055	.0033
15	.0067	.0027	.0042	.0049

TABLE I: KL-divergence of the approximate joint PDF of  $R_1$  and  $R_2$  computed as the product of their marginal PDFs from their empirical joint PDF.

$$+ \int_0^{\frac{r_1}{2}} F_{W_1,2}(r_1 - x_1 | \mathcal{E}_{0,1}, x_1) \mathbb{P}(\mathcal{E}_{0,1} | X_1) f_{X_1}(x_1) dx_1 + \mathbb{P}(\mathcal{E}_{1,1}) F_{R_1}(r_1 | \mathcal{E}_{1,1}). \quad (16)$$

*Proof.* The CDF of  $R_1$  can be computed as

$$\begin{aligned} F_{R_1}(r_1) &= \mathbb{P}(R_1 < r_1) \\ &\stackrel{(a)}{=} \mathbb{P}(R_1 < r_1, \mathcal{E}_{0,1}) + \mathbb{P}(R_1 < r_1, \mathcal{E}_{1,1}) \\ &= \mathbb{E}_{X_1} [\mathbb{P}(R_1 < r_1, \mathcal{E}_{0,1} | X_1)] + \mathbb{P}(R_1 < r_1, \mathcal{E}_{1,1}) \\ &\stackrel{(b)}{=} \mathbb{E}_{X_1} [\mathbb{P}(R_1 < r_1 | \mathcal{E}_{0,1}, X_1) \mathbb{P}(\mathcal{E}_{0,1} | X_1)] + \mathbb{P}(R_1 < r_1 | \mathcal{E}_{1,1}) \mathbb{P}(\mathcal{E}_{1,1}) \\ &= \int_0^\infty \mathbb{P}(x_1 + W_1 < r_1 | \mathcal{E}_{0,1}, X_1) \mathbb{P}(\mathcal{E}_{0,1} | X_1) f_{X_1}(x_1) dx_1 + \mathbb{P}(\mathcal{E}_{1,1}) \mathbb{P}(R_1 < r_1 | \mathcal{E}_{1,1}) \\ &= \int_0^\infty F_{W_1}(r_1 - x_1 | \mathcal{E}_{0,1}, x_1) \mathbb{P}(\mathcal{E}_{0,1} | X_1) f_{X_1}(x_1) dx_1 + \mathbb{P}(\mathcal{E}_{1,1}) F_{R_1}(r_1 | \mathcal{E}_{1,1}) \\ &\stackrel{(c)}{=} \int_0^{\frac{r_1}{2}} F_{W_1,1}(r_1 - x_1 | \mathcal{E}_{0,1}, x_1) \mathbb{P}(\mathcal{E}_{0,1} | X_1) f_{X_1}(x_1) dx_1 \\ &\quad + \int_0^{\frac{r_1}{2}} F_{W_1,2}(r_1 - x_1 | \mathcal{E}_{0,1}, x_1) \mathbb{P}(\mathcal{E}_{0,1} | X_1) f_{X_1}(x_1) dx_1 + \mathbb{P}(\mathcal{E}_{1,1}) F_{R_1}(r_1 | \mathcal{E}_{1,1}), \end{aligned}$$

where (a) follows from the law of total probability, (b) follows from the application of Bayes' theorem, and (c) follows from substituting (10) in the previous step.  $\square$

In order to compute the exact CDF of  $\min\{R_1, R_2\}$ , we need to determine the joint distribution of  $R_1$  and  $R_2$ , which is not quite tractable due to the peculiar coupling induced by the underlying line process. Therefore, in the interest of analytical tractability, we assume  $R_1$  and  $R_2$  to be independent and derive the approximate CDF of  $\min\{R_1, R_2\}$ . This assumption is strongly supported by the empirical evidence obtained from Monte-Carlo simulations. For different sets of  $\lambda_l$  and  $\lambda_c$ , we determined the Kullback-Leibler (KL) divergence of the approximate joint PDF of  $R_1$  and  $R_2$  computed as the product of their marginal PDFs from their actual joint PDF, as shown in Table I. It can be observed that the KL divergence for different combinations of  $\lambda_l$  and  $\lambda_c$  is quite small. Thus, we can infer that the dependence between  $R_1$  and  $R_2$  is minimal. So, using the assumption of independence between  $R_1$  and  $R_2$ , we derive an approximate lower bound for the CDF of  $R_m$  in the following theorem.

**Theorem 2.** *For the typical point located at some arbitrary position on the line  $L_x$ , the CDF of  $R_m$  is approximately lower bounded by*

$$F_{R_m}(r_m) \gtrsim 1 - (1 - F_{R_1}(r_m))^2, \quad (17)$$

where  $F_{R_1}(\cdot)$  is the marginal distribution of  $R_1$  given in Lemma 5.

*Proof.* The CDF of  $R_m$  can be computed as

$$\begin{aligned} F_{R_m}(r_m) &= \mathbb{P}(R_m < r_m) \\ &\geq \mathbb{P}(\min\{R_1, R_2\} < r_m) \\ &= 1 - \mathbb{P}(R_1 > r_m, R_2 > r_m) \\ &\stackrel{(a)}{\approx} 1 - \mathbb{P}(R_1 > r_m) \mathbb{P}(R_2 > r_m) \end{aligned}$$

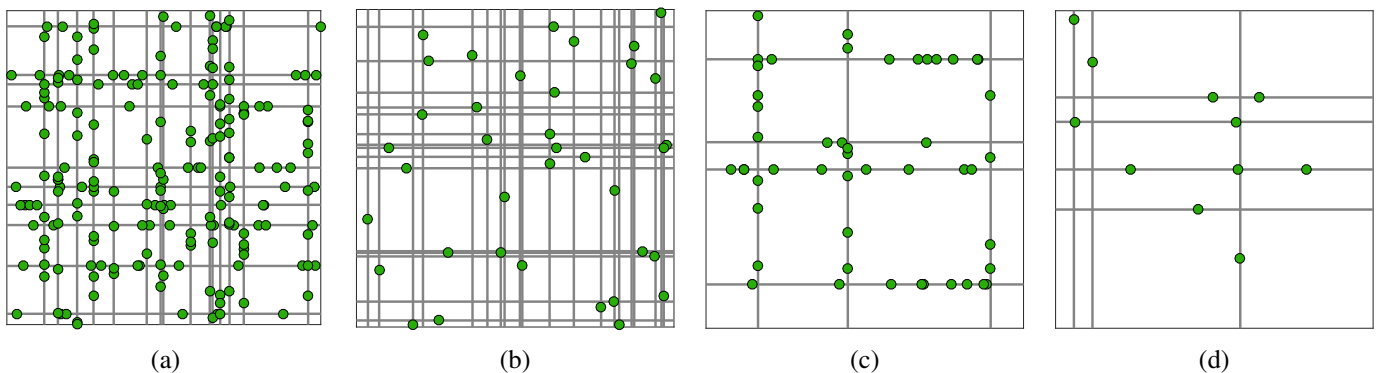


Fig. 9: The four different regimes of the spatial model: (a) Dense lines - dense points (DL-DP), (b) Dense lines - sparse points (DL-SP), (c) Sparse lines - dense points (SL-DP), and (d) Sparse lines - sparse points (SL-SP).

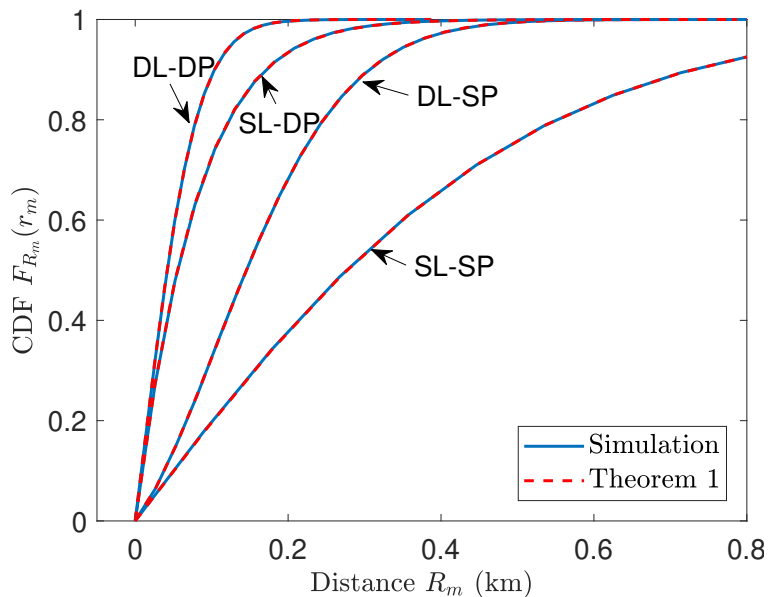


Fig. 10: CDF of the minimum shortest path distance for the typical point at the intersection for the four regimes: DL-DP ( $\lambda_l = 10 \text{ km}^{-1}$ ,  $\lambda_c = 3 \text{ points/km}$ ), SL-DP ( $\lambda_l = 1 \text{ km}^{-1}$ ,  $\lambda_c = 3 \text{ points/km}$ ), DL-SP ( $\lambda_l = 10 \text{ km}^{-1}$ ,  $\lambda_c = 0.5 \text{ points/km}$ ), and SL-SP ( $\lambda_l = 1 \text{ km}^{-1}$ ,  $\lambda_c = 0.5 \text{ points/km}$ ).

$$\stackrel{(b)}{=} 1 - (1 - F_{R_1}(r_m))^2,$$

where (a) follows from assuming  $R_1$  and  $R_2$  to be independent, and (b) follows from the identical distribution of  $R_1$  and  $R_2$ . This completes the proof.  $\square$

#### IV. RESULTS AND DISCUSSION

In this section, we will present the numerical results and discuss some of the applications of these results in transportation networks, infrastructure planning and wireless networks.

##### A. Numerical results

We first compute the empirical CDF of  $R_m$  using Monte-Carlo simulations and compare it with the CDF obtained from the analytical expressions given in Theorems 1 and 2. In order to visualize the effectiveness of the bounds proposed in this paper, we evaluate the results under four broad regimes based on the densities of lines and points: (i) dense lines - dense points (DL-DP) corresponding to large values of  $\lambda_l$  and  $\lambda_c$ , (ii) dense lines - sparse

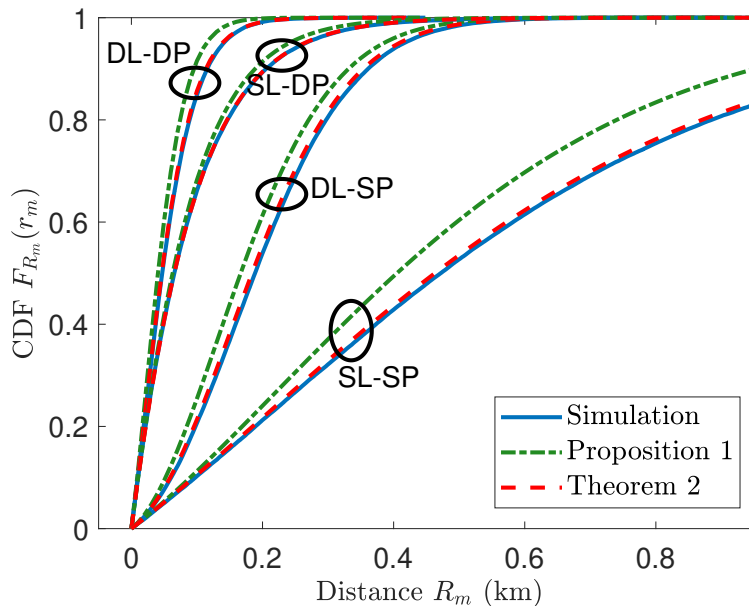


Fig. 11: CDF of the minimum shortest path distance for the typical point located at an arbitrary position for the four regimes: DL-DP ( $\lambda_l = 10 \text{ km}^{-1}$ ,  $\lambda_c = 5 \text{ points/km}$ ), SL-DP ( $\lambda_l = 1 \text{ km}^{-1}$ ,  $\lambda_c = 5 \text{ points/km}$ ), DL-SP ( $\lambda_l = 10 \text{ km}^{-1}$ ,  $\lambda_c = 0.5 \text{ points/km}$ ), and SL-SP ( $\lambda_l = 1 \text{ km}^{-1}$ ,  $\lambda_c = 0.5 \text{ points/km}$ ).

points (DL-SP) corresponding to large values of  $\lambda_l$  and small values of  $\lambda_c$ , (iii) sparse lines - dense points (SL-DP) corresponding to small values of  $\lambda_l$  and large values of  $\lambda_c$ , and (iv) sparse lines - sparse points (SL-SP) corresponding to small values of  $\lambda_l$  and  $\lambda_c$ , as illustrated in Fig. 9. Note that Fig. 9 is only for illustration purpose and the actual simulation values corresponding to these configurations are provided along with the results in Figs. 10 and 11. For the typical point located at an intersection, as expected, the CDF obtained from the expression in (2) matches exactly with the empirical CDF for all the configurations as depicted in Fig. 10. For the typical point located at some arbitrary position on a line, while the upper bound given in Proposition 1 is not extremely tight in all the regimes, the approximate lower bound given in Theorem 2 closely follows the empirical CDF, as shown in Fig. 11. The remarkable accuracy of the lower bound follows from the careful construction of two approximately independent random variables  $R_1$  and  $R_2$ , as discussed in detail in Section III.

### B. Applications to other areas

1) *Wireless communication*: As we have mentioned in Section I, the MPLCP can be used to model the locations of vehicular nodes and roadside units (RSUs) in a vehicular network and analyze key performance metrics such as coverage and rate by leveraging the Euclidean distance properties. However, in the case of millimeter wave communications in an urban environment, the high frequency radio signals suffer from severe attenuation upon propagating through the buildings and the dominant component of the signal is often the one that travels along the roads with diffractions around the corners at intersections [34]. As a result, the analytical techniques developed in this paper can be leveraged to characterize the propagation delays and the received power of such signals. This is quite useful in deriving the power-delay profile of the wireless channel which is an important exercise in the performance analysis of wireless networks.

2) *Transportation systems and Infrastructure planning*: In transportation networks, the spatial layout of roads can be modeled by MPLP and the various places of interest such as gas stations or charging stations for electric vehicles can be modeled by a MPLCP. Thus, the length of the shortest path studied in the paper can be viewed as the shortest distance that needs to be traveled by a vehicular user to reach the nearest destination of a certain type. Building further on the results presented in this paper, it is possible to analytically characterize the distance-dependent cost metrics that are of interest in transportation systems such as minimum travel time and fuel consumption. These results can be useful in characterizing the response time of medical or police personnel to arrive at the site of an emergency. Such analyses can also provide macroscopic insights into urban planning and design.



## V. CONCLUSION

In this paper, we have focused on the analytical characterization of the shortest path distance in a stationary MPLCP. For this spatial model, we first derived the closed-form expression for the CDF of the shortest path distance between the typical point located at the intersection and its closest point in the sense of path distance. Building on this result, we derived an upper bound and a much tighter but approximate lower bound for the CDF of the shortest path distance for the typical point located at some arbitrary position. We then discussed some useful applications of our results in wireless communication networks, transportation networks, infrastructure planning and personnel deployment.

This work has several extensions. First of all, the spatial model considered in the paper can be used to study other useful metrics such as route-length efficiency statistic which is defined as a function of the ratio of the shortest path distance between a pair of points to the corresponding Euclidean distance between those points [35]. While we have derived the results for a MPLCP, the analytical procedure and the construction of bounds can be extended to a PLCP. Also, the discussion on applications of our results in transportation, infrastructure planning, and wireless communication in Section IV-B could motivate future work in all these areas.

## REFERENCES

- [1] M. Barthélemy, "Spatial networks," *Physics Reports*, vol. 499, no. 1-3, pp. 1–101, 2011.
- [2] D. Aldous and P. Diaconis, "Hammersley's interacting particle process and longest increasing subsequences," *Probability Theory and Related Fields*, vol. 103, no. 2, pp. 199–213, June 1995.
- [3] S. Mertens and C. Moore, "Continuum percolation thresholds in two dimensions," *Phys. Rev. E*, vol. 86, p. 061109, Dec. 2012.
- [4] C. P. Dettmann and O. Georgiou, "Random geometric graphs with general connection functions," *Phys. Rev. E*, vol. 93, p. 032313, Mar. 2016.
- [5] H. Hilhorsta, "Statistical properties of planar Voronoi tessellations," *The European Physical Journal B*, vol. 64, no. 3-4, pp. 437–441, 2008.
- [6] K. Koufos and C. P. Dettmann, "Distribution of cell area in bounded Poisson Voronoi tessellations with application to secure local connectivity," *Journal of Statistical Physics*, vol. 176, no. 5, pp. 1296–1315, 2019.
- [7] S. Goudsmit, "Random distribution of lines in a plane," *Reviews of Modern Physics*, vol. 17, no. 2-3, p. 321, 1945.
- [8] H. Hilhorst and P. Calka, "Random line tessellations of the plane: statistical properties of many-sided cells," *Journal of Statistical Physics*, vol. 132, no. 4, pp. 627–647, 2008.
- [9] C. Dodson and W. Sampson, "Planar line processes for void and density statistics in thin stochastic fibre networks," *Journal of Statistical Physics*, vol. 129, no. 2, pp. 311–322, 2007.
- [10] J. Tykesson and D. Windisch, "Percolation in the vacant set of Poisson cylinders," *Probability theory and related fields*, vol. 154, no. 1-2, pp. 165–191, 2012.
- [11] S. N. Chiu, D. Stoyan, W. S. Kendall, and J. Mecke, *Stochastic geometry and its applications*. John Wiley & Sons, 2013.
- [12] R. E. Miles, "Random polygons determined by random lines in a plane," *Proceedings of the National Academy of Sciences*, vol. 52, no. 4, pp. 901–907, 1964.
- [13] R. E. Miles, "Random polygons determined by random lines in a plane, II," *Proceedings of the National Academy of Sciences*, vol. 52, no. 5, pp. 1157–1160, 1964.
- [14] R. E. Miles, "The various aggregates of random polygons determined by random lines in a plane," *Advances in Mathematics*, vol. 10, no. 2, pp. 256–290, 1973.
- [15] M. Bartlett, "The spectral analysis of line processes," in *Proc. Fifth Berkeley Symp. Math. Statist. Probab*, vol. 3, 1967, pp. 135–152.
- [16] R. Davidson, "Construction of line processes: Second order properties," *Izv. Akad. Nauk. Armjan. SSR Ser. Mat*, vol. 5, pp. 219–34, 1970.
- [17] A. Fairclough and G. Davies, "Poisson line processes in 2 space to simulate the structure of porous media: Methods of generation, statistics and applications," *Chemical Engineering Communications*, vol. 92, no. 1, pp. 23–48, 1990.
- [18] A. Rosenfeld and L. S. Davis, "Image segmentation and image models," *Proceedings of the IEEE*, vol. 67, no. 5, pp. 764–772, May 1979.
- [19] T. Meyer and H. H. Einstein, "Geologic stochastic modeling and connectivity assessment of fracture systems in the boston area," *Rock Mechanics and Rock Engineering*, vol. 35, no. 1, pp. 23–44, Feb. 2002.
- [20] F. Baccelli, M. Klein, M. Lebourges, and S. Zuyev, "Stochastic geometry and architecture of communication networks," *Telecommunication Systems*, vol. 7, no. 1, pp. 209–227, June 1997.
- [21] C. Gloaguen, F. Fleischer, H. Schmidt, and V. Schmidt, "Analysis of shortest paths and subscriber line lengths in telecommunication access networks," *Networks and Spatial Economics*, vol. 10, no. 1, pp. 15–47, Mar. 2010.
- [22] S. Aditya, H. S. Dhillon, A. F. Molisch, and H. Behairy, "Asymptotic blind-spot analysis of localization networks under correlated blocking using a Poisson line process," *IEEE Wireless Commun. Letters*, vol. 6, no. 5, pp. 654–657, Oct. 2017.
- [23] F. Voss, C. Gloaguen, F. Fleischer, and V. Schmidt, "Distributional properties of Euclidean distances in wireless networks involving road systems," *IEEE Journal on Sel. Areas in Commun.*, vol. 27, no. 7, pp. 1047–1055, Sep. 2009.
- [24] C. Gloaguen, F. Fleischer, H. Schmidt, and V. Schmidt, "Simulation of typical Cox Voronoi cells with a special regard to implementation tests," *Mathematical Methods of Operations Research*, vol. 62, no. 3, pp. 357–373, 2005.
- [25] C. Gloaguen, F. Fleischer, H. Schmidt, and V. Schmidt, "Fitting of stochastic telecommunication network models via distance measures and Monte-Carlo tests," *Telecommunication Systems*, vol. 31, no. 4, pp. 353–377, Apr. 2006.

- [26] V. V. Chetlur and H. S. Dhillon, "Coverage analysis of a vehicular network modeled as cox process driven by poisson line process," *IEEE Trans. on Wireless Commun.*, vol. 17, no. 7, pp. 4401–4416, July 2018.
- [27] V. V. Chetlur and H. S. Dhillon, "Coverage and rate analysis of downlink cellular vehicle-to-everything (C-V2X) communication," *IEEE Trans. on Wireless Commun.*, to appear.
- [28] V. V. Chetlur and H. S. Dhillon, "Success probability and area spectral efficiency of a VANET modeled as a Cox process," *IEEE Wireless Commun. Letters*, vol. 7, no. 5, pp. 856–859, Oct. 2018.
- [29] C. Choi and F. Baccelli, "An analytical framework for coverage in cellular networks leveraging vehicles," *IEEE Trans. on Commun.*, vol. 66, no. 10, pp. 4950–4964, Oct. 2018.
- [30] C. Choi and F. Baccelli, "Poisson Cox point processes for vehicular networks," *IEEE Trans. on Veh. Technology*, vol. 67, no. 10, pp. 10 160–10 165, Oct. 2018.
- [31] F. Voss, C. Gloaguen, and V. Schmidt, "Scaling limits for shortest path lengths along the edges of stationary tessellations," *Advances in Applied Probability*, vol. 42, no. 4, pp. 936–952, 2010.
- [32] M. Haenggi, *Stochastic Geometry for Wireless Networks*. Cambridge University Press, 2013.
- [33] F. Morlot, "A population model based on a Poisson line tessellation," in *Proc., Modeling and Optimization in Mobile, Ad Hoc and Wireless Networks*, May 2012, pp. 337–342.
- [34] Y. Wang, K. Venugopal, A. F. Molisch, and R. W. Heath, "MmWave vehicle-to-infrastructure communication: Analysis of urban microcellular networks," *IEEE Trans. on Veh. Technology*, vol. 67, no. 8, pp. 7086–7100, Aug. 2018.
- [35] D. J. Aldous and J. Shun, "Connected spatial networks over random points and a route-length statistic," *Statist. Sci.*, vol. 25, no. 3, pp. 275–288, Aug. 2010.